Journal of Industrial and Engineering Chemistry 34 (2016) 66–75

Contents lists available at ScienceDirect

Journal of Industrial and Engineering Chemistry

journal homepage: www.elsevier.com/locate/jiec

Effect of side chain position and conformation of quinacridone–quinoxaline based conjugated polymers on photovoltaic properties

Kyu Hyo Hwang, Doo Hun Kim, Min Hee Choi, Jae Pil Han, Doo Kyung Moon *

Department of Materials Chemistry and Engineering, Konkuk University, 1 Hwayang-dong, Gwangjin-gu, Seoul 143-701, Republic of Korea

ARTICLE INFO

Article history:
Received 31 July 2015
Received in revised form 8 October 2015
Accepted 24 October 2015
Available online 30 October 2015

Keywords:
Quinacridone
Quinoxaline
Side-chain
Suzuki coupling reaction
Bulk heterojunction polymer solar cells

ABSTRACT

Poly[quinacridone-*alt*-dithienylquinoxaline](PQCDTQx)s series with alkoxy chains at different anchoring positions (*meta*- or *para*-) in quinoxaline were synthesized *via* Suzuki coupling reaction. The ICT effects were stronger at the *meta* than *para*. Meta-polymers had enhanced π–π stacking of the polymer main chains and showed a lower HOMO energy level than those of the *para*, from −5.26 to −5.16 eV, because of the greater electron-withdrawing effects of the alkoxy groups. As a result, the photovoltaic device comprising a PQCDTQx-mEH/$PC_{71}BM$ (1:4) blend system exhibited performance, with a PCE, J_{SC}, V_{OC}, and FF of 2.1%, 4.8 mA/cm^2, 0.73 V, and 59.3%, respectively.

Introduction

Polymer solar cells (PSCs) have recently received much attention, because they use an unlimited amount of photovoltaic energy, which is reproducible. And they offer many advantages, such as low production costs, lightweight, flexibility and suitability to large-scale production. Bulk heterojunction (BHJ) systems, combining conjugated polymers as the electron donors and fullerene derivatives as the electron acceptors, have played a significant role in enhancing the photovoltaic performance of PSCs. Therefore, BHJ PSCs have been the subject of diverse studies [1–5]. The formation of a donor–acceptor (D–A) system by the alternate copolymerization of an electron-donating unit (D) and electron-accepting unit (A) is a typical method for designing the molecular structures of conjugated polymers for high-efficiency BHJ PSCs. An appropriate selection of these D and A building blocks can be used to effectively tune the energy levels of PSCs [6].

The use of quinacridone (QC) as an electron-donating unit is well known, because of its red–violet pigments, ordered structure, self-assembly characteristics, and high hole mobility. It has been increasingly used in organic thin-film transistors (OTFTs) [7,8]. The Takimiya group reported the use of a polymer composed of QC derivatives with a high hole mobility (0.2 cm^2/V S) in OTFTs [9].

Quinoxaline (Qx) derivatives are widely used as the electron-accepting units owing to their superior electron-withdrawing properties, caused by the presence of two imine nitrogens. The structural modification of Qx derivatives has been readily achieved by using a variety of substituents to change their solubility and electronic properties [10–12].

An understanding of the correlation between the molecular structure and the device performance is also important for the production of high-efficiency PSCs. The open-circuit voltage (V_{OC}), short-circuit current density (J_{SC}), and fill factor (FF) play important roles in determining the power conversion efficiency (PCE) of PSCs. V_{OC} is determined from the difference between the lowest unoccupied molecular orbital (LUMO) of the electron acceptor and the highest occupied molecular orbital (HOMO) of the electron donor, i.e., the difference in their electron affinities. Therefore, the HOMO level of the polymer donor is an important factor in determining the PCE [13]. A previous study reported the tuning of the HOMO and LUMO levels of conjugated polymers by changing their electron affinities according to the positions of the side chains introduced, while retaining the same polymer backbone repeating unit [14]. Takimiya et al. reported an enhancement in the photovoltaic properties by determining its exciton diffusion, charge separation, and charge transport properties by using the effect of the type of side chain used on a polymer's crystallinity and backbone orientation [15]. Moreover, Wang et al. demonstrated a maximum PCE of 5% using a thiophene–quinoxaline (TQ)-based alternating copolymer to

* Corresponding author. Tel.: +82 2 450 3498; fax: +82 2 444 0765.
E-mail address: dkmoon@konkuk.ac.kr (D.K. Moon).

http://dx.doi.org/10.1016/j.jiec.2015.10.029
1226-086X/

study its aggregation, orientation, and phase behavior as a function of side chain type [16].

In this study, the deep HOMO levels and backbone orientations of polymers were observed according to the position and form of the Qx side chain and the morphological changes caused by the miscibility of Qx with 1-(3-methoxycarbonyl)propyl-1-phenyl-[6,6]-C71($PC_{71}BM$). In order to accomplish these characteristics, different QC-Qx-based conjugated polymers, poly[quinacridone-*alt*-dithienyl-(3-octyloxy phenyl)quinoxaline] (PQCDTQx-m8), poly[quinacridone-*alt*-dithienyl-(3-(2-ethylhexyloxy phenyl)quinoxaline] (PQCDTQx-mEH), poly[quinacridone-*alt*-dithienyl-(4-octyloxy phenyl)quinoxaline] (PQCDTQx-p8), and poly[quinacridone-*alt*-dithienyl-(4-(2-ethylhexyl)phenyl)quinoxaline] (PQCDTQx-pEH), were synthesized by introducing two types of side chains (linear octyl or branched 2-ethylhexyl) at two different phenyl ring positions (*meta*- or *para*-) on Qx. By UV–visible (UV–vis) spectroscopy, an absorption shoulder peak (λ_{sh}) was identified at the *meta* position of the polymer in both the solution and thin-film states. Moreover, the HOMO and LUMO energy levels of the resulting polymers were regulated according to the differences in the electron-donating abilities caused by the position of the alkoxy side chain. The backbone orientations of the polymers, according to the positions and conformations of the side chains, were confirmed by X-ray diffraction (XRD) measurements. When PQCDTQx-mEH was used as the donor polymer, the best photovoltaic performance (PCE = 2.1%) was achieved at PQCDTQx-mEH:$PC_{71}BM$ (1:4, w/w).

Results and discussion

Synthesis and characterization of polymers

Scheme 1 shows the chemical structures of the monomers and polymers used, along with their synthetic processes. The relevant monomers (Qx derivatives) used in this study were synthesized by introducing two types of side chains (linear octyl or branched 2-ethylhexyl) onto the *meta*- and *para*-positions of the phenyl ring according to the previously reported procedures [27–29]. Thiophene was introduced as the conjugated linker on the acceptor unit to synthesize 5,8-bis(5-bromothiophen-2-yl)-2,3-bis(3-(octyloxy)phenyl)quinoxaline (M2), 5,8-bis(5-bromothiophen-2-yl)-2,3-bis(3-(2-ethylhexyloxy)phenyl)quinoxaline (M3), 5,8-bis(5-bromothiophen-2-yl)-2,3-bis(4-(octyloxy)phenyl)quinoxaline (M4), and 5,8-bis(5-bromothiophen-2-yl)-2,3-bis(4-(2-ethylhexyloxy)-phenyl)quinoxaline (M5) according to the procedures as described in Scheme 1. As shown in Scheme 1, poly[quinacridone-*alt*-dithienyl-quinoxaline] (PQCDTQx-m8, PQCDTQx-mEH, PQCDTQx-p8, and PQCDTQx-pEH) was synthesized via the Suzuki coupling reaction of 2,9-diboronicester-*N*,*N*′-di (2-octyl-dodecyl)quinacridone (M1) and M2 through M5. The polymerization of the three polymers, PQCDTQx-m8, PQCDTQx-p8, and PQCDTQx-pEH, was performed for 24 h at 90–95 °C using toluene, $Pd(PPh_3)_4$(0), a 2 M aqueous potassium carbonate solution, and Aliquat 336 as the solvent, catalyst, base, and surfactant, respectively. However, because of its low solubility, PQCDTQx-mEH was polymerized for 48 h using toluene/DMF (9:1) as the solvent. After polymerization was completed, the polymers were end-capped with bromothiophene. The polymers were then recovered by precipitation in methanol. Purification was performed using a Soxhlet extraction, sequentially with methanol, acetone, and chloroform. Finally, the polymers were recovered by precipitating the chloroform fraction in methanol. As a result, the yields of PQCDTQx-m8, PQCDTQx-mEH, PQCDTQx-p8, and PQCDTQx-pEH were 89, 88, 51, and 91%, respectively. The derived polymers dissolved easily in common organic solvents such as tetrahydrofuran (THF), chloroform, chlorobenzene, and *o*-dichlorobenzene, forming homogeneous violet semitransparent films after spin coating. The structures of the synthesized polymers were confirmed via ^{1}H NMR spectroscopy (see the electronic Supplemental information (ESI), Fig. S1) and elemental analysis (EA).

Table 1 shows the measured molecular weights of the polymers; As shown in Table 1, PQCDTQx-m8, PQCDTQx-mEH, PQCDTQx-p8, and PQCDTQx-pEH exhibited number average molecular weights (M_n) of 112, 113, 197, and 129 kDa, respectively, and polydispersity indices (PDIs) of 2.10, 2.01, 2.32, and 2.53, respectively. Thermogravimetric analysis (TGA) was used to evaluate the thermal stability of the polymers, and the TGA results are shown in the ESI (Fig. S2). According to the TGA results, the temperature at which a 5% thermal weight loss occurred in N_2 atmosphere was >340 °C for all the polymers. All the synthesized polymers exhibited good thermal stability, and their suitability for device fabrication and application was verified.

Optical properties

To examine the effects of side chain position on the optoelectronic properties of QC–Qx-based polymers, normalized UV–vis absorption spectra of the polymers in both the solution and thin-film states are shown in Fig. 1, and the results are summarized in Table 2. As indicated in Fig. 1, all the polymers displayed two absorption peaks between 300 and 800 nm. The peak in the high-energy region (300–450 nm) was owing to the π–π^* transitions of the donor segments (QC group), whereas the peak in the low-energy region (450–700 nm) was caused by an intramolecular charge transfer (ICT) transition between the donor and acceptor [17,18]. The maximum absorption peaks of PQCDTQx-m8 and PQCDTQx-mEH in solution were 399 and 555 nm (λ_{sh} = 600 nm), and 402 and 555 nm (λ_{sh} = 600 nm), respectively, while those for PQCDTQx-p8 and PQCDTQx-pEH appeared at 393 and 544 nm, and 393 and 545 nm, respectively. The absorption coefficient calculated from the maximum absorption peak (λ_{max}) of each polymer in the solution was 7.0×10^4, 7.8×10^4, 8.2×10^4, and 6.7×10^4 M^{-1} cm^{-1} for PQCDTQx-m8, PQCDTQx-mEH, PQCDTQx-p8, and PQCDTQx-pEH, respectively. The maximum absorption peaks of PQCDTQx-m8 and PQCDTQx-mEH in the thin film were 399, 575 nm (λ_{sh} = 607 nm), and 399, 571 nm (λ_{sh} = 593 nm) respectively and these values red-shifted by 20 and 16 nm, respectively, in comparison to the solution-state results. PQCDTQx-p8 and PQCDTQx-pEH displayed peaks at 393, 541 nm (λ_{sh} = 579 nm), and 393, 551 nm (λ_{sh} = 585 nm), respectively, and were similar to the peaks observed in solution. The occurrence of a red shift in the thin-film state could have been caused by the aggregation and π–π intermolecular interactions of the polymer main chains, which were stronger in the solid state [19,20]. Accordingly, because the polymers in the *meta* position showed a greater red-shift, stronger polymer main chain aggregation and more ordered π–π stacking occurred to induce more effective intermolecular interactions, enabling smaller optical band gaps to be obtained from the absorption occurring in a broader region of the spectrum. Moreover, when the side chain was introduced in the *meta* position (PQCDTQx-m8 and PQCDTQx-mEH), shoulder peaks appeared in both the solution (λ_{sh} = 600 nm) and thin-film (λ_{sh} = 607 and 593 nm) states, because polymers in the *meta* position have strong aggregation and excellent π–π stacking even in dilute solutions [21,22]. When the side chains were introduced in the *para* position (PQCDTQx-p8 and PQCDTQx-pEH), shoulder peaks were not observed in solution; however, absorption shoulder peaks at 579 and 585 nm were observed in the thin-film state, respectively. The position of side chain attachment affected the stacking properties, polymer chain interaction, and UV–vis absorption region. However, no significant difference in the UV–vis spectra was observed by the type of side chain [30]. The calculation of the optical band gaps (E_g^{opt}) of the four polymers

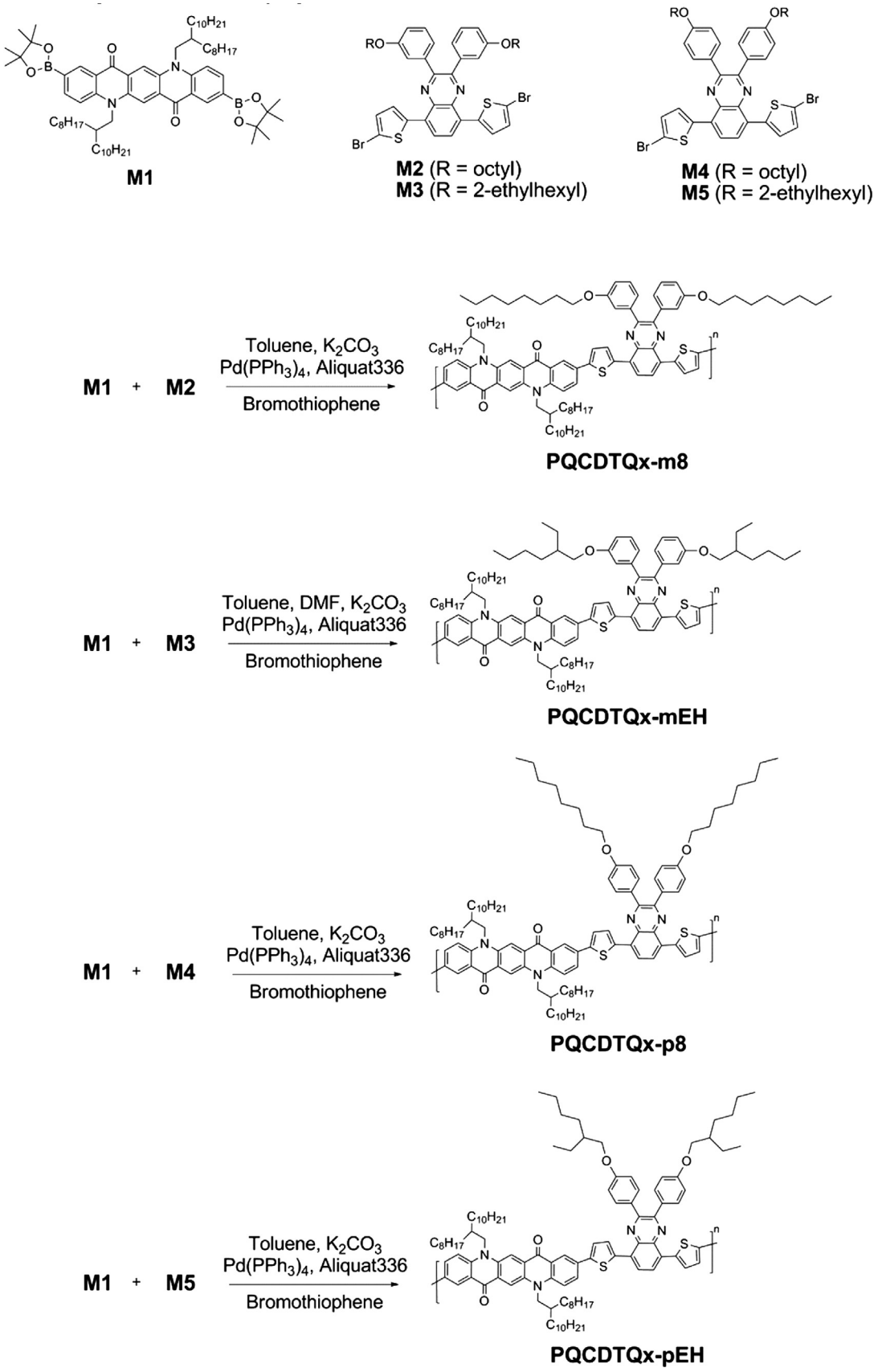

Scheme 1. Synthetic route to polymers.

Table 1
Physical and thermal properties of polymers.

Polymer	Yield [%]	M_n[a] [kDa]	M_w[a] [kDa]	PDI[a]	T_d[b] [°C]
PQCDTQx-m8	89	112	238	2.10	382
PQCDTQx-mEH	88	113	229	2.01	435
PQCDTQx-p8	51	197	460	2.32	355
PQCDTQx-pEH	91	129	328	2.53	341

[a] Determined by GPC in chloroform ($CHCl_3$) using polystyrene standards.
[b] Temperature resulting in 5% weight loss based on the initial weight.

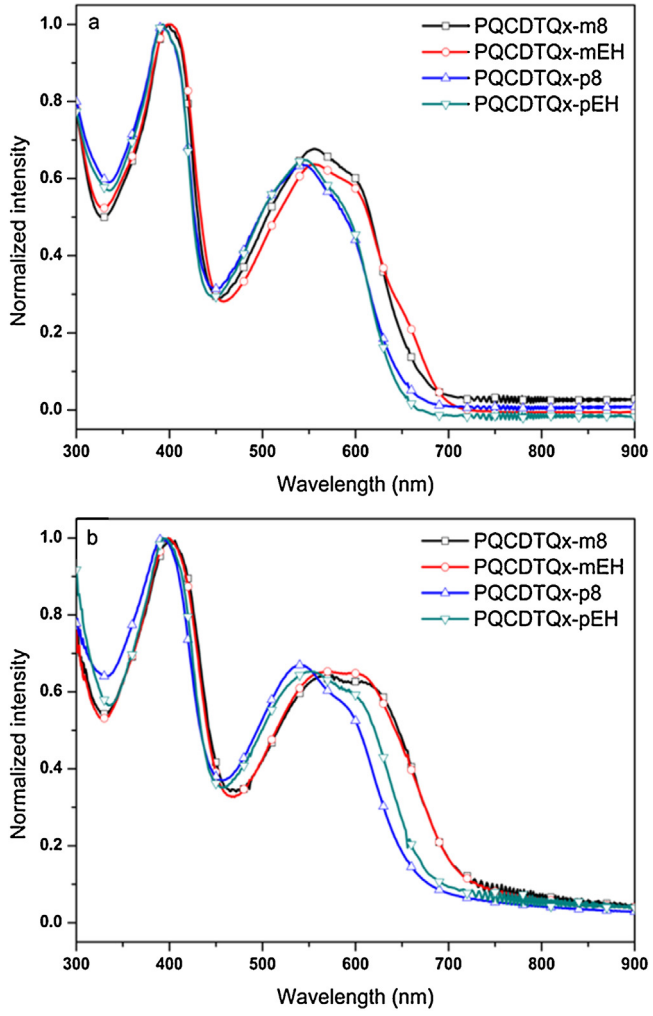

Fig. 1. UV–vis absorption spectra of polymers in (a) solution and (b) film.

from the absorption onset (λ_{onset}) of the solid-state film via the band edge revealed that PQCDTQx-m8 and PQCDTQx-mEH had the same E_g^{opt} of 1.74 eV, whereas the E_g^{opt} of PQCDTQx-p8 and PQCDTQx-pEH were 1.87 and 1.83 eV, respectively.

Electrochemical properties

Cyclic voltammograms (CVs) were used to determine the electronic energy levels of the polymer films. Measurements were taken in a 0.1 M tetrabutylammonium-hexafluorophosphate acetonitrile solution, and the results are shown in Fig. 2 and Table 2. As shown in Fig. 2 and Table 2, the oxidation onset potentials (E_{ox}^{onset}) of PQCDTQx-m8, PQCDTQx-mEH, PQCDTQx-p8, and PQCDTQx-pEH were +0.85, +0.88, +0.79, and +0.80 V, while the HOMO levels were −5.23, −5.26, −5.17, and −5.18 eV, respectively. The LUMO levels were calculated from the difference between the HOMO levels and E_g^{opt}, resulting in LUMO levels at −3.49, −3.52, −3.30, and −3.35 eV for PQCDTQx-m8, PQCDTQx-mEH, PQCDTQx-p8, and PQCDTQx-pEH, respectively. When the side chain was introduced in the *para* position, the HOMO and LUMO levels tended to be higher than those in the *meta* position. These findings were consistent with that reported by Hou et al. indicating that an alkoxy group showed greater electron-donating effects in the *para* position than in the *meta* position [14]. You et al. reported that the HOMO energy level were dependent on the donor strength in the push–pull system [32]. Therefore, the introduction of a side chain on the *meta* position increased electron-donating property for higher HOMO and LUMO values. In addition, according to the difference of the type of side chain, 2-ethylhexyl side chains exhibited slightly higher HOMO levels than the *n*-octyl side chains. These results are in good agreement with the branched side chains stabilized HOMO as a function of structural bulkiness [33].

Theoretical calculations

To understand the electrical properties of the synthesized polymers, density functional theory (DFT) was used to simulate the distribution of the electronic density of states (Fig. S3), molecular geometries, and dihedral angles (Fig. 3 and Table 3). DFT calculations were performed using Gaussian 09 with a hybrid B3LYP correlation function and a split valence 6-31G(d) basis set. For simplification of the computations, the polymer backbones were modeled as oligomers with a single repeating unit. The calculated HOMO (LUMO) energy level values of PQCDTQx-m8, PQCDTQx-mEH, PQCDTQx-p8, and PQCDTQx-pEH were −4.84 eV (−2.13 eV), −4.84 eV (−2.14 eV), −4.82 eV (−2.12 eV), and −4.84 eV (−2.12 eV), respectively. These values were similar because of the similarities in the structures of the main polymer backbones. However, the calculated HOMO and LUMO energy level of PQCDTQx-p8, and PQCDTQx-pEH had a tendency to upshift. Moreover, these results are in agreement with the CV data.

Table 2
Optical and electrochemical properties of polymers.

Polymer	UV–vis absorption					E_g^{opt}[a] [eV]	Cyclic voltammetry		
	$CHCl_3$ solution		Film				E_{ox}^{onset} [V]	HOMO[b] [eV]	LUMO[b] [eV]
	λ_{max} [nm]	λ_{sh} [nm]	λ_{max} [nm]	λ_{sh} [nm]	λ_{onset} [nm]				
PQCDTQx-m8	399, 555	600	399, 575	607	709	1.74	0.85	−5.23	−3.49
PQCDTQx-mEH	402, 555	600	399, 571	593	709	1.74	0.88	−5.26	−3.52
PQCDTQx-p8	393, 544	–	393, 541	579	663	1.87	0.79	−5.17	−3.30
PQCDTQx-pEH	393, 545	–	393, 551	585	677	1.83	0.80	−5.18	−3.35

[a] Calculated from the intersection of the tangent on the low energetic edge of the absorption spectrum with the baseline.
[b] $E_{HOMO\ (or\ LUMO)} = -[E_{onset}(\text{vs Ag/AgCl}) - E_{1/2}(Fc/Fc^{+}\ \text{vs Ag/AgCl})] - 4.8$ eV.

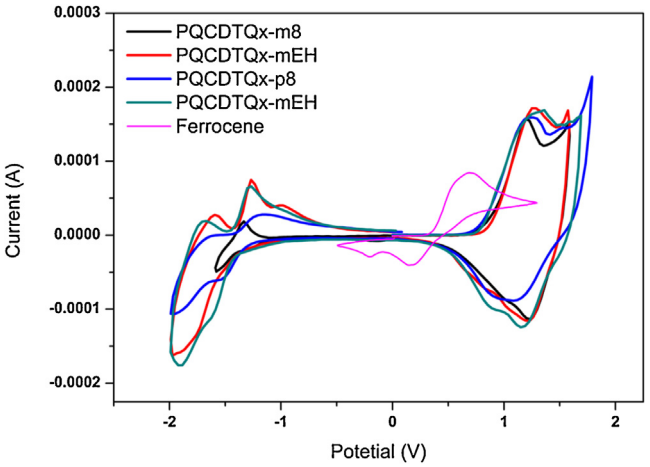

Fig. 2. Cyclic voltammograms of polymers.

In Fig. S3, the polymers' HOMO was delocalized on the polymer main chains. However, the LUMO had different localized forms that were determined by the location of the side chain introduced on the acceptor. For the LUMO in the *meta* position, the electron clouds were localized up to the acceptor's core, including Qx and the spacer. This localization was because of the structural characteristics of the nonbinding electron pairs of the nitrogen and quinoid formed on the bottom of the benzene ring [23,24]. However, the LUMO of the polymers with a side chain in the *para* position were localized at QC, the donor, more than at Qx, the acceptor. This localization might result from the *para* position side chain. Qx had a relatively weaker electron-withdrawing property than QC. These findings were consistent with the findings of Biwu Ma et al., indicating that the QC core can act as a donor or an acceptor under different conditions, depending on the electron affinity of the attached units [25]. In other words, it was shown that when an alkoxy group was introduced as a side chain in the *para* position, Qx was nearly unable to act as an electron acceptor.

Fig. 3(a) shows a side view of the optimized geometries of the polymer backbones and the schematic diagram of the backbones according to their dihedral angles. The side view of the *meta*-polymers showed a planar configuration of the polymer backbones, and the side chain introduced on the phenyl ring of Qx was also extended parallel to the polymer backbone. However, the *para*-polymers showed a low planarity, caused by tilting the polymer backbone. The angles between the main chain and side chain attached to Qx were 13.6 and 15.0° in PQCDTQx-m8 and

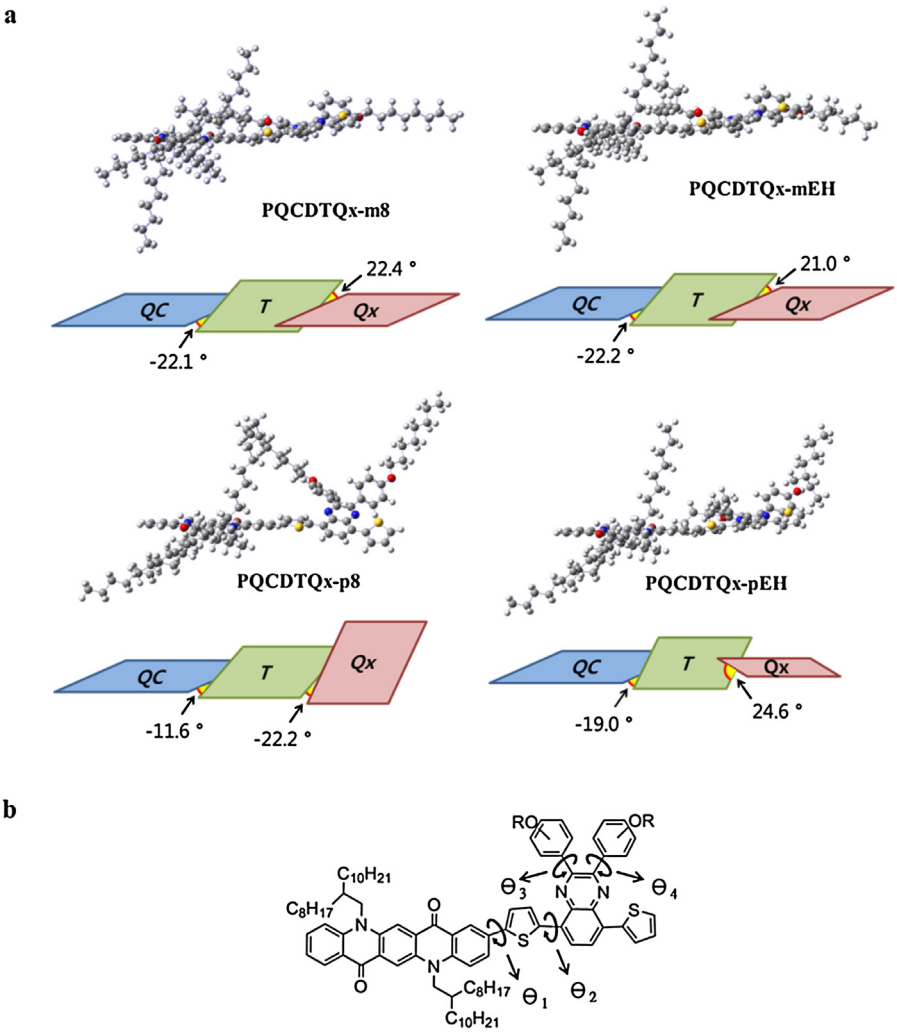

Fig. 3. (a) Side view of the optimized geometries of the backbone of polymers and schematic diagram of polymer backbones by dihedral angles; chain length $n = 1$; color code: gray (C), white (H), red (O), blue (N) and yellow (S). (b) Dihedral angles of polymers. (For interpretation of the references to color in this figure legend, the reader is referred to the web version of this article.)

Table 3
Calculated dihedral angles of polymers.

Polymers	Dihedral angle (deg)			
	θ_1	θ_2	θ_3	θ_4
PQCDTQx-m8	−22.1	22.4	37.5	39.4
PQCDTQx-mEH	−22.2	21.0	39.1	38.6
PQCDTQx-p8	11.6	22.2	37.4	37.1
PQCDTQx-pEH	−19.0	24.6	35.9	38.3

PQCDTQx-mEH, respectively, whereas these angles were 33.2 and 65.9° in PQCDTQx-p8 and PQCDTQx-pEH, respectively.

In the schematic diagram shown in Fig. 3(a), the dihedral angles between QC and thiophene (θ_1) were −22.1 and −22.2° for PQCDTQx-m8 and PQCDTQx-mEH, respectively, whereas the dihedral angles between Qx and thiophene (θ_2) were 22.4 and 21.0°. Because the angle between the QC and Qx cores, excluding the spacer, was offset to ~0°, the overall planarity of the main chain was maintained. However, the values of θ_1 were 11.6 and −19.0° for PQCDTQx-p8 and PQCDTQx-pEH, respectively, whereas the values of θ_2 were 22.2 and 24.6°. Because PQCDTQx-p8 had positive values for both θ_1 and θ_2, the angle between the QC and Qx cores increased, affecting the planarity.

Therefore, the *meta* position had a more planar structure than the *para* position in a manner that was consistent with the previous results, demonstrating an enhanced intermolecular π−π stacking in the *meta*-polymers from their UV–vis spectra. The dihedral angles of the polymers are shown in Fig. 3(b) and Table 3. All the polymers displayed similar dihedral angles for their phenyl rings, indicating that the structural changes based on the side chain position occurred primarily on the polymer backbone without significantly affecting the inside of the acceptor unit.

XRD measurements

To gain a better understanding of the ordering and crystallinity of the thin-film polymers as a function of side chain type and position, XRD measurements were performed at annealing temperatures.

Fig. 4(a) shows the XRD results for the polymer films measured in the out-of-plane. Each polymer displayed two diffraction peaks in the out-of-plane mode, indicating that the polymers formed both the (h 0 0) lamellar structures and (0 h 0) lamellar structures. At the (1 0 0) position, PQCDTQx-m8, PQCDTQx-mEH, PQCDTQx-p8, and PQCDTQx-pEH showed peaks at 3.81, 3.90, 3.69, and 3.84°, respectively. These angles were used to calculate the ordered (1 0 0) lamellar d-spacing (d_1) via Bragg's law ($\lambda = 2d\sin\theta$), resulting in the d_1 values of 23.16, 22.62, 23.91, and 22.98 Å for PQCDTQx-m8, PQCDTQx-mEH, PQCDTQx-p8, and PQCDTQx-pEH, respectively. Moreover, PQCDTQx-m8, PQCDTQx-mEH, PQCDTQx-p8, and PQCDTQx-pEH displayed wider peaks at the (0 1 0)

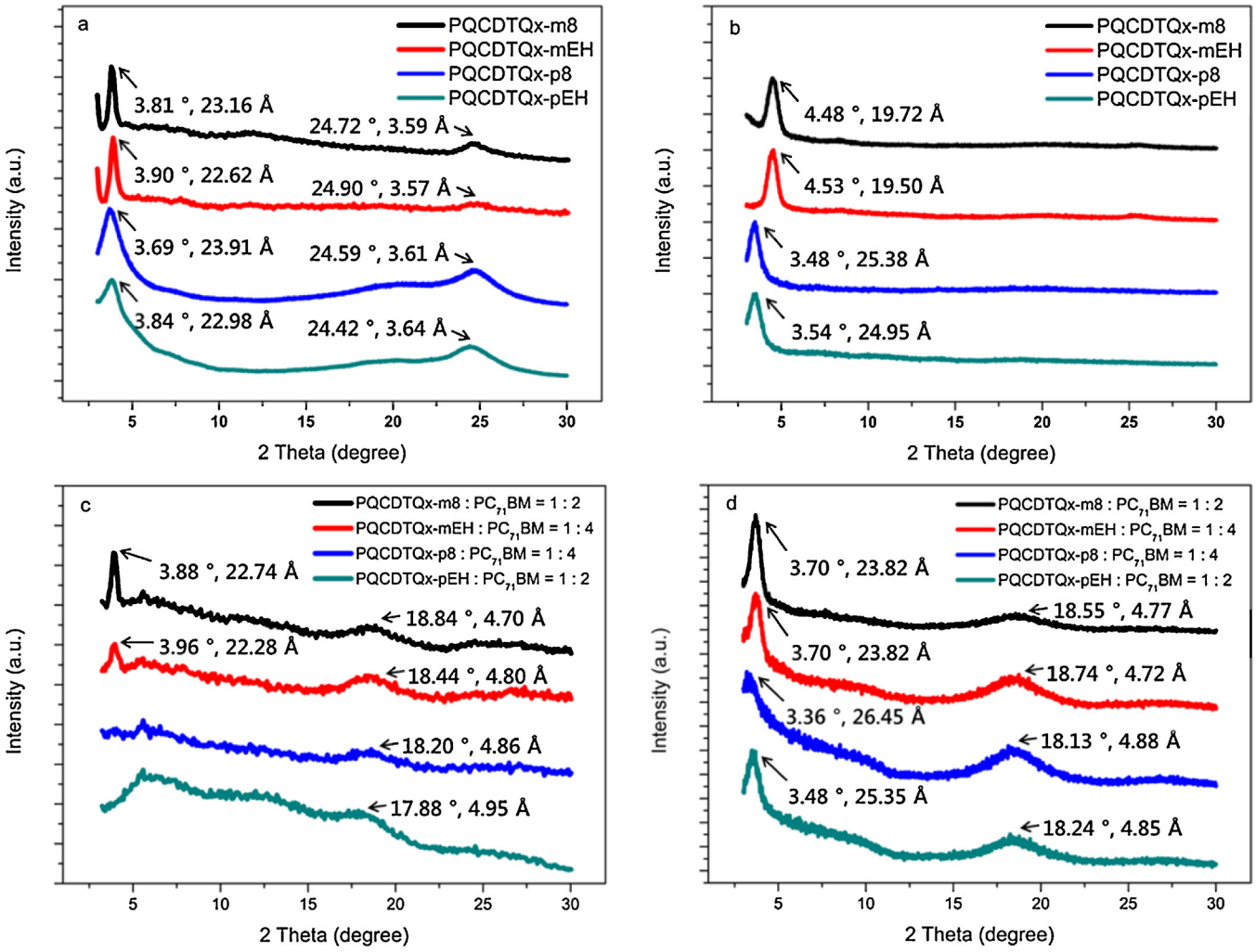

Fig. 4. X-ray diffraction pattern of polymers on a silicon wafer and a polymer: $PC_{71}BM$ blend on silicon wafer out-of-plane mode (a and c) and in-plane mode (c and d).

position with the angles of 24.72, 24.90, 24.59, and 24.42°, respectively. These values were used to calculate the intermolecular π−π stacking distances (d_π) of 3.59, 3.57, 3.61, and 3.64 Å for PQCDTQx-m8, PQCDTQx-mEH, PQCDTQx-p8, and PQCDTQx-pEH, respectively. The d_π-spacing of PQCDTQx-m8 and PQCDTQx-mEH were shorter than those of PQCDTQx-p8 and PQCDTQx-pEH. These results well matched with the UV–vis absorption spectra in that the polymers with *meta* position side chain showed a shoulder peak in both the solution and thin-film states. As shown Fig. 4(a), when π−π stacking was observed on the (0 1 0) plane in the out-of-plane mode, the crystalline structure inside the polymer film might have formed a face-on orientation, which was identified by the in-plane mode XRD measurement. Fig. 4(b) shows the XRD results for the polymer films measured in the in-plane mode. For all the polymers, peaks were only observed at low angles, demonstrating that all the polymers had face-on crystallites [15].

Fig. 4(c) and (d) show the out-of-plane and in-plane modes XRD measurements of the polymer/$PC_{71}BM$ blended thin films. Fig. 4(c) shows that the (1 0 0) peaks disappeared when PQCDTQx-p8 and PQCDTQx-pEH were compared to the pristine polymer films. The loss of the (1 0 0) peaks could have been caused by a decrease in the crystallinity of the *para*-polymers' (h 0 0) lamellar structure when blended with $PC_{71}BM$. Moreover, the *meta*-polymers displayed distinctive (1 0 0) peaks similar to those of the pristine polymer film. The XRD results of the $PC_{71}BM$ blended thin films measured in the in-plane mode are shown in Fig. 4(d); PQCDTQx-m8, PQCDTQx-mEH, PQCDTQx-p8, and PQCDTQx-pEH displayed peaks at 18.84, 18.44, 18.20, and 17.88°, respectively, because of the crystallinity of $PC_{71}BM$.

Photovoltaic properties and morphology analysis

To investigate the photovoltaic properties of the synthesized polymers, conventional BHJ PSCs were fabricated. The photovoltaic properties of the polymers were measured by fabricating PSC devices with an ITO/PEDOT:PSS/polymer:$PC_{71}BM$/Al structure. The fabricated devices were encapsulated in a glove box. Their current densities vs. voltage (*J*–*V*) characteristics were measured in an ambient atmosphere with an active area of 7 mm^2. The weight ratios of polymer/$PC_{71}BM$ were between 1:1 (w/w) and 1:4 (w/w), using ~0.5–1 wt% concentrations of *o*-dichlorobenzene (*o*-DCB) as the solvent. Optimized conditions were achieved with 1 wt% *o*-DCB at a ratio of 1:2 for PQCDTQx-m8 and PQCDTQx-pEH and with 0.5 wt% *o*-DCB at a ratio of 1:4 for PQCDTQx-mEH and PQCDTQx-p8. The *J*–*V* curves of the polymers at their optimized weight ratios are shown in Fig. 5(a), and the IPCE at the time of measurement is shown in Fig. 5(b). The photovoltaic properties of the fabricated PSCs are listed in Table 4.

Table 4
Photovoltaic properties of polymers.

Polymer	$PC_{71}BM$ ratios	V_{OC} [V]	J_{SC} [mA/cm^2]	FF [%]	PCE [%]
PQCDTQx-m8	1:2	0.70	5.3	52.5	2.0
PQCDTQx-mEH	1:4	0.73	4.8	59.3	2.1
PQCDTQx-p8	1:4	0.67	3.9	59.1	1.7
PQCDTQx-pEH	1:2	0.68	3.4	58.9	1.5

PQCDTQx-m8/$PC_{71}BM$ (1:2) had a V_{OC}, J_{SC}, and FF of 0.70 V, 5.3 mA/cm^2, and 52.5%, respectively, resulting in an equivalent PCE of 2.0%. Meanwhile, PQCDTQx-mEH/$PC_{71}BM$ (1:4) had a V_{OC}, J_{SC}, and FF of 0.73 V, 4.8 mA/cm^2, and 59.3%, respectively, and an equivalent PCE of 2.1%. PQCDTQx-p8/$PC_{71}BM$ (1:4) had a V_{OC}, J_{SC}, FF, and PCE of 0.67 V, 3.9 mA/cm^2, 59.1%, and 1.7%, respectively. PQCDTQx-pEH/$PC_{71}BM$ (1:2) had a V_{OC}, J_{SC}, FF, and PCE of 0.68 V, 3.4 mA/cm^2, 58.9%, and 1.5%, respectively. The introduction of the side chain in the *meta* position resulted in higher J_{SC} values than those achieved with the side chains in the *para* position, because side chains in the *meta* position have strong π−π stacking interactions as observed in the UV–vis spectra of the polymer films. This finding is consistent with the more effective intermolecular interactions indicated by the shoulder peak in the UV–vis spectra and XRD diffraction patterns.

The surface morphologies of the polymer blends were also critical in determining the efficiencies of the PSCs. Therefore, the morphologies of the polymer/$PC_{71}BM$ films were observed using atomic force microscopy (AFM), and the results are shown in Fig. 6. The dark- and light-colored areas correspond to $PC_{71}BM$ and polymer domains, respectively. The thicknesses of all types of polymers/$PC_{71}BM$ films were in the range ~60–70 nm. The surfaces of the PQCDTQx-m8 and PQCDTQx-mEH/$PC_{71}BM$ blended films were smooth with nanoscale features and low root-mean-square (RMS) roughnesses of 2.79 and 0.94 nm, respectively. Intermixing between the polymers and $PC_{71}BM$ occurred, allowing the formation of prominent polymer channels, which was consistent with the high J_{SC} of the two polymers. Conversely,

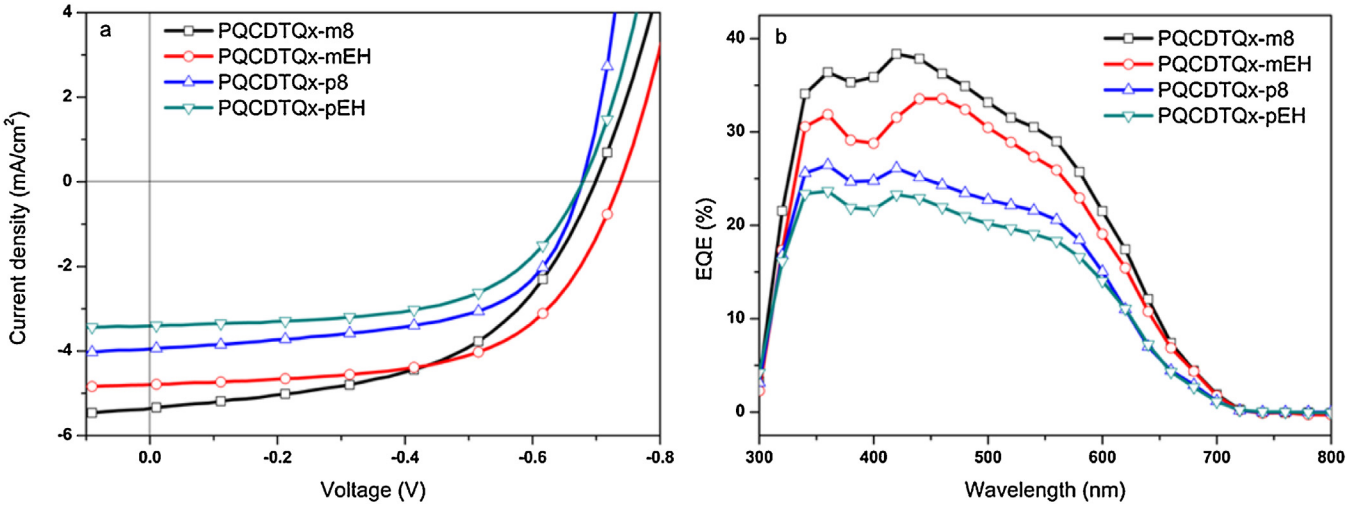

Fig. 5. The *J*–*V* curves of the PSC based on polymer: $PC_{71}BM$ (a) under the illumination of AM 1.5G, 100 mW/cm^2. The IPCE spectra of the PSC based on polymer: $PC_{71}BM$ (b).

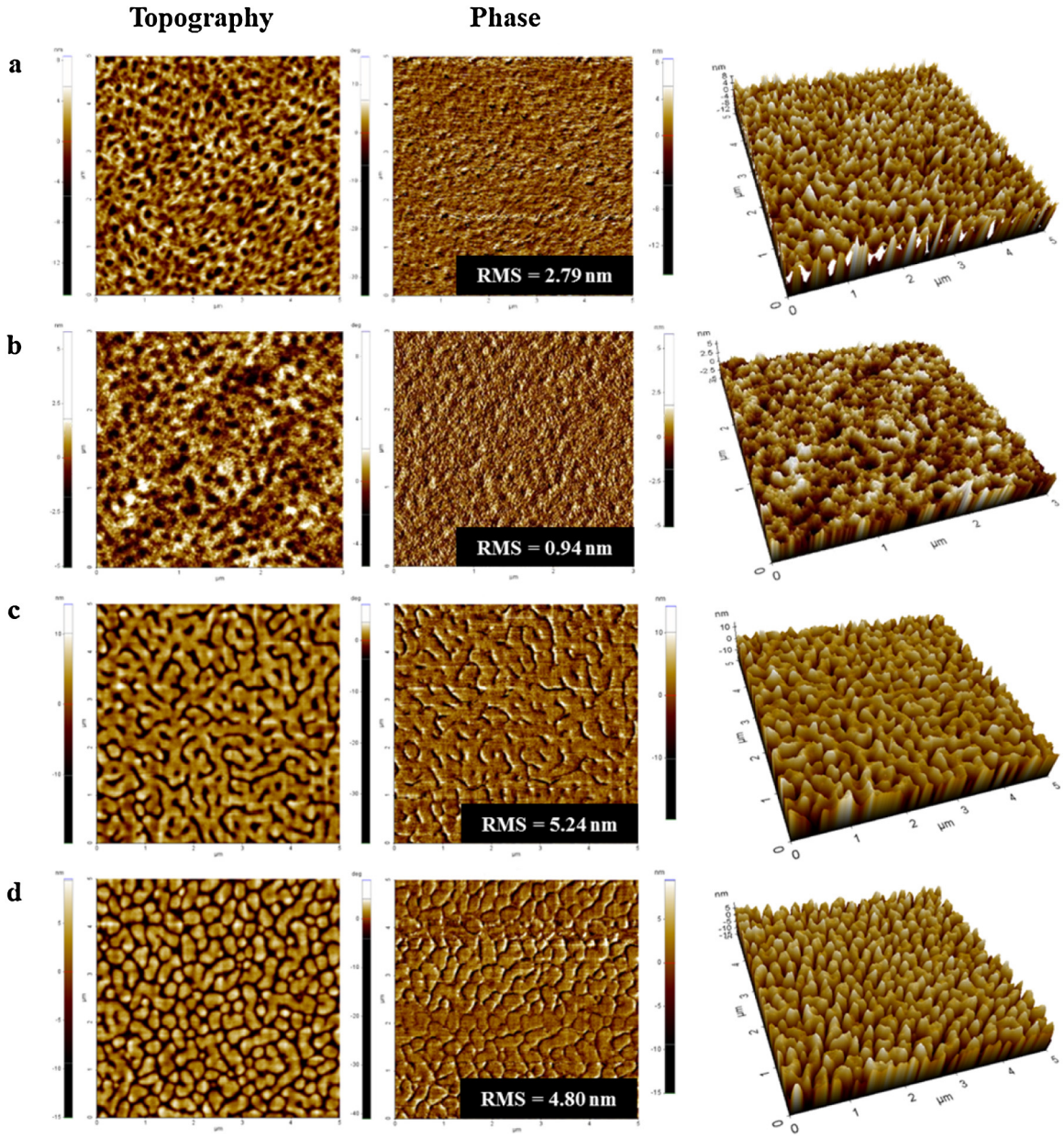

Fig. 6. Topographic AFM images ($5 \times 5\ \mu m^2$) of (a) PQCDTQx-m8: $PC_{71}BM$ = 1: 2, (b) PQCDTQx-mEH: $PC_{71}BM$ = 1: 4, (c) PQCDTQx-p8: $PC_{71}BM$ = 1: 4, (d) PQCDTQx-pEH: $PC_{71}BM$ = 1: 2.

the separation of macrophases because of the highly aggregated $PC_{71}BM$ domains was observed for PQCDTQx-p8 and PQCDTQx-pEH/$PC_{71}BM$ blended thin films, and these surfaces were rougher with the RMS roughnesses of 5.24 and 4.80 nm, respectively. The smoother blend film based on the *meta*-polymers may effectively reduce charge recombination and traps [31]. This is the reason why PQCDTQx-p8 and PQCDTQx-pEH had a low J_{SC} and EQE, though PQCDTQx-p8 showed the highest absorption coefficient in the UV–vis spectra. The RMS roughness of the *para*-polymers was higher than those of the *meta*-polymers, because steric hindrance with $PC_{71}BM$ increased the tilting of the main chain according to the dihedral angle of the polymer backbone, as mentioned previously alongside the DFT calculations [4,23]. PQCDTQx-m8 and PQCDTQx-mEH formed smaller domains than PQCDTQx-p8 and PQCDTQx-pEH. Therefore, exciton dissociation and carrier collection efficiency enhanced to provide higher J_{SC} values [26]. V_{OC} was higher for the *meta*-polymers than for the *para*-polymers and was consistent with the HOMO levels measured by CV.

Conclusions

In this study, Suzuki coupling reaction was used to successfully synthesize four types of poly[quinacridone-*alt*-dithienyl-quinoxaline], PQCDTQx-m8, PQCDTQx-mEH, PQCDTQx-p8, and PQCDTQx-pEH, according to the position and structure of the side chain. The polymers with the side chain introduced in the *meta* position exhibited more effective ICT effects on the UV–vis absorption, whereas the *meta*-polymers demonstrated a stronger stacking capability as evidenced by the shoulder absorption peaks in solution. Dihedral angles were calculated via DFT, indicating that the improved $\pi-\pi$ stacking was because of the higher planarity of the *meta*-structures. Moreover, the electron affinity of Qx, the acceptor unit, changed depending on whether an alkoxy group was positioned at the *meta*- or *para*-, indicating that electron localization in the LUMO electron distribution appeared differently according to DFT. From these calculations, the electronic properties of the polymers were found to be regulated by modifying the positions of

the polymers' side chains. Consequently, the *meta*-polymers exhibited superior J_{SC} values than those of the *para*-polymers, resulting in higher PCEs. Among the polymers studied, PQCDTQx-mEH/$PC_{71}BM$ (1:4, w/w) showed the best performance with a PCE, V_{OC}, J_{SC}, and FF of 2.1%, 0.73 V, 4.8 mA/cm^2, and 59.3%, respectively.

Experimental

Materials

All the starting materials were purchased from Sigma-Aldrich, Acros, Alfar Aesar, or TCI companies and used without further purification. Toluene and tetrahydrofuran (THF) were distilled from benzophenone ketyl and sodium. The following compounds were synthesized following the modified literature procedures: 2,9-diboronicester-*N,N′*-di(2-octyldodecyl)quinacridone (M1) [27], 5,8-bis(5-bromothiophen-2-yl)-2,3-bis(3-(octyloxy)phenyl)-quinoxaline (M2) [28], 5,8-bis(5-bromothiophen-2-yl)-2,3-bis (3-(2-ethylhexyloxy)phenyl)quinoxaline (M3) [28], 5,8-bis(5-bromothiophen-2-yl)-2,3-bis(4-(octyloxy)phenyl)quinoxaline (M4) [29], 5,8-bis(5-bromothiophen-2-yl)-2,3-bis(4-(2-ethylhexyloxy)-phenyl)quinoxaline (M5) [29].

Poly[quinacridone-alt-*dithienyl-2,3-bis(3-octyloxy)quinoxaline] (PQCDTQx-m8)*

5,8-Bis(5-bromothiophen-2-yl)-2,3-bis(3-(octyloxy)phenyl)-quinoxaline (M2) (0.131 g, 0.15 mmol), 2,9-diboronicester-*N,N′*-di(2-octyl-dodecyl)quinacridone (M1) (0.171 g, 0.15 mmol), $Pd(PPh_3)_4(0)$ (0.005 g, 0.0045 mmol), and Aliquat336 were placed in a Schlenk tube, purged with three nitrogen/vacuum cycles, and 2 M degassed aqueous K_2CO_3 (7.5 mL) and anhydrous toluene (15 mL) were added under a nitrogen atmosphere. The mixture was heated to 90 °C and stirred for 24 h. After the polymerization was completed, the polymer was end-capped with bromothiophene. After quenching the reaction, the reaction mixture was poured in methanol. The precipitate was filtered off and purified by Soxhlet extraction with solvents in the order methanol, acetone, and chloroform. The polymer was recovered from the chloroform fraction and precipitated in methanol. The final product was obtained as a dark violet solid after drying in vacuum (0.211 g, 89%). ^{1}H NMR ($CDCl_3$) d (ppm): 8.5–8.3 (br, 4*H*), 8.3–8.1 (br, 2*H*), 8.0–7.73 (br, 4*H*), 7.70–7.5 (br, 6*H*), 7.48–7.32 (6*H*), 7.0 (2*H*), 4.15 (br, 4*H*), 3.95 (br, 4*H*), 2.23 (br, 2*H*), 1.57–1.1 (br, 88*H*), 0.83 (br, 18*H*). Anal. calcd. For: $C_{104}H_{140}N_4O_4S_2$: C, 79.34; H, 8.96; N, 3.56; O, 4.06; S, 4.07. Found: C, 78.98; H, 8.84; N, 3.64; O, 4.12; S, 4.11%.

Poly[quinacridone-alt-*dithienyl-2,3-bis(3-(2-ethylhexyloxy)quinoxaline] (PQCDTQx-mEH)*

5,8-Bis(5-bromothiophen-2-yl)-2,3-bis(3-(2-ethylhexyloxy)-phenyl)quinoxaline (M3) (0.172 g, 0.20 mmol), 2,9-diboronicester-*N,N′*-di(2-octyl-dodecyl)quinacridone (M1) (0.225 g, 0.20 mmol), $Pd(PPh_3)_4(0)$ (0.007 g, 0.006 mmol), and Aliquat336 were placed in a Schlenk tube, purged with three nitrogen/vacuum cycles, and under a nitrogen atmosphere, 2 M degassed aqueous K_2CO_3 (10 mL), anhydrous toluene (18 mL), and DMF (2 mL) were added. The mixture was heated to 105 °C and stirred for 48 h. After the polymerization completed, the polymer was end-capped with bromothiophene. After quenching the reaction, the reaction mixture was poured in methanol. The precipitate was filtered off and purified by Soxhlet extraction with solvents in the order methanol, acetone and chloroform. The polymer was recovered from the chloroform fraction and precipitated into methanol. The final product was obtained as a dark violet solid after drying in vacuum (0.28 g, 88%). ^{1}H NMR ($CDCl_3$) d (ppm): 8.5–8.32 (br, 4*H*), 8.3–8.15 (br, 2*H*), 7.84–7.74 (br, 4*H*), 7.74–7.63 (br, 6*H*), 7.49–7.41 (6*H*), 6.99 (2*H*), 3.92 (br, 4*H*), 3.77 (br, 4*H*), 2.01 (br, 2*H*), 1.57–1.1 (br, 88*H*), 0.83 (br, 18*H*). Anal. calcd. For: $C_{104}H_{140}N_4O_4S_2$: C, 79.34; H, 8.96; N, 3.56; O, 4.06; S, 4.07. Found: C, 79.23; H, 8.25; N, 3.58; O, 4.92; S, 3.98%.

Poly[quinacridone-alt-*dithienyl-2,3-bis(4-octyloxy)quinoxaline] (PQCDTQx-p8)*

5,8-Bis(5-bromothiophen-2-yl)-2,3-bis(4-(octyloxy)phenyl)-quinoxaline (M4) (0.23 g, 0.27 mmol), 2,9-diboronicester-*N,N′*-di(2-octyl-dodecyl)quinacridone (M1) (0.30 g, 0.27 mmol), $Pd(PPh_3)_4(0)$ (0.009 g, 0.008 mmol), and Aliquat336 were placed in a Schlenk tube, purged with three nitrogen/vacuum cycles, and 2 M degassed aqueous K_2CO_3 (10 mL) and anhydrous toluene (20 mL) were added under a nitrogen atmosphere. The mixture was heated to 90 °C and stirred in the dark for 24 h. After the polymerization completed, the polymer was end-capped with bromothiophene. After quenching the reaction, the reaction mixture was poured in methanol. The precipitate was filtered off and purified by Soxhlet extraction with solvents in the order methanol, acetone and chloroform. The polymer was recovered from the chloroform fraction and precipitated into methanol. The final product was obtained as a dark violet solid after drying in vacuum (0.23 g, 51%). ^{1}H NMR ($CDCl_3$) d (ppm): 8.1–7.92 (br, 4*H*), 7.9–7.65 (br, 2*H*), 7.51 (br, 4*H*), 7.39–7.32 (br, 6*H*), 7.13 (6*H*), 6.99 (2*H*), 4.85 (br, 4*H*), 4.32 (br, 4*H*), 2.05 (br, 2*H*), 1.57–1.1 (br, 88*H*), 0.83 (br, 18*H*). Anal. calcd. For: $C_{104}H_{140}N_4O_4S_2$: C, 79.34; H, 8.96; N, 3.56; O, 4.06; S, 4.07. Found: C, 79.22; H, 9.03; N, 3.56; O, 4.09; S, 4.05%.

Poly[quinacridone-alt-*dithienyl-2,3-bis(4-(2-ethylhexyloxy)quinoxaline] (PQCDTQx-pEH)*

5,8-Bis(5-bromothiophen-2-yl)-2,3-bis(4-(2-ethylhexyloxy)-phenyl)quinoxaline (M5) (0.23 g, 0.27 mmol), 2,9-diboronicester-*N,N′*-di(2-octyl-dodecyl)quinacridone (M1) (0.30 g, 0.27 mmol), $Pd(PPh_3)_4(0)$ (0.009 g, 0.008 mmol), and Aliquat336 were placed in a Schlenk tube, purged with three nitrogen/vacuum cycles, and 2 M degassed aqueous K_2CO_3 (10 mL) and anhydrous toluene (20 mL) were added under a nitrogen atmosphere. The mixture was heated to 90 °C and stirred in the dark for 24 h. After the polymerization was over, the polymer was end-capped with bromothiophene. After quenching, the reaction mixture was poured in methanol. The precipitate was filtered off and purified by Soxhlet extraction with solvents in the order methanol, acetone and chloroform. The polymer was recovered from the chloroform fraction and precipitated into methanol. The final product was obtained as a dark violet solid after drying in vacuum (0.39 g, 91%). ^{1}H NMR ($CDCl_3$) d (ppm): 8.5–8.3 (br, 4*H*), 8.3–8.2 (br, 2*H*), 8.07–7.93 (br, 4*H*), 7.9–7.7 (br, 6*H*), 7.65–7.04(6*H*), 7.18–7.01 (2*H*), 4.2 (br, 4*H*), 3.94 (br, 4*H*), 2.26 (br, 2*H*), 1.57–1.1 (br, 88*H*), 0.83 (br, 18*H*). Anal. calcd. for $C_{104}H_{140}N_4O_4S_2$: C, 79.34; H, 8.96; N, 3.56; O, 4.06; S, 4.07. Found: C, 78.72; H, 8.96; N, 3.20; O, 4.07; S, 4.08%.

Measurements

^{1}H NMR (400 MHz) spectra were recorded using a Brüker AMX400spectrometer in $CDCl_3$, and the chemical shifts were recorded in ppm with TMS as the internal standard. The absorption spectra were recorded using an Agilent 8453 UV–vis spectroscopy system. The solutions that were used for the UV–vis spectroscopy measurements were dissolved in chloroform at a concentration of 10 μg/mL. The films were drop-coated from the chloroform solution onto a quartz substrate. All the GPC analyses were performed using $CHCl_3$ as the eluent and polystyrene standard as the reference. The TGA measurements were performed using a TG 209 F3 thermogravimetric analyzer. The cyclic voltammetric waves were produced using a Zahner IM6eX electrochemical workstation with a 0.1 M acetonitrile (substituted with nitrogen for 20 min) solution containing tetrabutylammonium hexafluorophosphate (Bu_4NPF_6) as the electrolyte at a constant scan rate of

50 mV/s. An ITO, a Pt wire, and a silver/silver chloride [Ag in 0.1 M KCl] were used as the working, counter, and reference electrodes, respectively. The electrochemical potential was calibrated against Fc/Fc^{+}. The HOMO levels of the polymers were determined using the oxidation onset value. Onset potentials were values obtained from the intersection of the two tangents drawn at the rising current and the baseline changing current of the CV curves. The LUMO levels were calculated from the differences between the HOMO energy levels and the optical band-gaps, which were determined by the UV–vis absorption onset values in the films. The current density–voltage (*J–V*) curves of the photovoltaic devices were measured using a computer-controlled Keithley 2400 source measurement unit (SMU) equipped with a Class A Oriel solar simulator under an illumination of AM 1.5G (100 mW/cm^2). The topographic images of the active layers were obtained by atomic force microscopy (AFM) in the tapping mode under ambient conditions using an XE-100 instrument.

Photovoltaic cell fabrication and treatment

All bulk-heterojunction PV cells were prepared using the following device fabrication procedure. The glass/indium tin oxide (ITO) substrates [Sanyo, Japan (10 Ω/γ)] were sequentially patterned lithographically, cleaned with detergent, ultrasonicated in deionized water, acetone, and isopropyl alcohol, dried on a hot plate at 120 °C for 10 min, and treated with oxygen plasma for 10 min to improve the contact angle just before film coating. Poly(3,4-ethylene-dioxythiophene):poly(styrene-sulfonate) (PEDOT:PSS, Baytron P 4083 Bayer AG) was passed through a 0.45-mm filter before being deposited on ITO at a thickness of ~32 nm by spin-coating at 4000 rpm in the air, and then dried at 120 °C for 20 min inside a glove box. A blend of 1-(3-methoxycarbonyl)propyl-1-phenyl-[6,6]-C71 ($PC_{71}BM$) and the polymer [~1:1–1:4 (w/w)] at a concentration of 7.5 mg/mL in *o*-DCB was stirred overnight, filtered through a 0.2-μm poly(tetrafluoroethylene) (PTFE) filter, and then spin coated (500–3000 rpm, 30 s) on the top of the PEDOT:PSS layer. The device was completed by the deposition of a 200-nm-thick aluminum layer at the pressures $<10^{-6}$ Torr. The active area of the device was 7 mm^2. Finally, the cell was encapsulated using UV-curing glue (Nagase, Japan).

Acknowledgments

This work was supported by the Energy Efficiency & Resources Core Technology Program of the Korea Institute of Energy Technology Evaluation and Planning (KETEP), granted financial resource from the Ministry of Trade, Industry & Energy, Republic of Korea (No. 20142020103970).

Appendix A. Supplementary data

Supplementary material related to this article can be found, in the online version, at doi:10.1016/j.jiec.2015.10.029.

References

[1] Min Hee Choi, Kwan Wook Song, Soo Won Heo, Yong Woon Han, Doo Kyung Moon, J. Ind. Eng. Chem. 26 (2015) 173.
[2] Hsiang-Yu Chen, Jianhui Hou, Shaoqing Zhang, Yongye Liang, Guanwen Yang, Yang Yang, Luping Yu, Yue Wu, Gang Li, Nat. Photonics 3 (2009) 649.
[3] Chil Won Lee, Oh Young Kim, Jun Yeob Lee, J. Ind. Eng. Chem. 20 (2014) 1198.
[4] Min-Hee Choi, Kwan Wook Song, Doo Kyung Moon, Polym. Chem 6 (2015) 2636.
[5] Kwan Wook Song, Min hee Choi, Myung hee Han, Doo Kyung Moon, J. Ind. Eng. Chem. 20 (2014) 426.
[6] Shu Liu, Xichang Bao, Wei Li, Kailong Wu, Guohua Xie, Renqiang Yang, Chuluo Yang, Macromolecules 48 (2015) 2948.
[7] Steven De Feyter, Andre Gesquiere, Frans C. De Schryver, Uwe Keller, Klaus Mullen, Chem. Mater. 14 (2002) 989.
[8] Xunyu Yang, Jia Wang, Xi Zhang, Zhiqiang Wang, Yue Wang, Langmuir 23 (2007) 1287.
[9] Itaru Osaka, Masahiro Akita, Tomoyuki Koganezawa, Kazuo Takimiya, Chem. Mater. 24 (2012) 1235.
[10] Ho-Jun Song, Doo-Hun Kim, Eui-Jin Lee, Doo-Kyung Moon, J. Mater. Chem. A 1 (2013) 6010.
[11] Kwan Wook Song, Tae Ho Lee, Eui Jin Ko, Kyung Hun Back, Doo Kyung Moon, J. Polym. Sci., A: Polym. Chem. 52 (2014) 1028.
[12] Ruomeng Duan, Long Ye, Xia Guo, Ye Huang, Peng Wang, Shaoqing Zhang, Jianping Zhang, Lijun Huo, Jianhui Hou, Macromolecules 45 (2012) 3032.
[13] Bong-Gi Kim, Xiao Ma, Chelsea Chen, Yutaka Ie, Elizabeth W. Coir, Hossein Hashemi, Yoshio Aso, Peter F. Green, John Keiffer, Jinsang Kim, Adv. Funct. Mater. 23 (2013) 439.
[14] Ye Huang, Mingqian Zhang, Long Ye, Xia Guo, Charles C. Han, Yongfang Li, Jianhui Hou, J. Mater. Chem. 22 (2012) 5700.
[15] Itaru Osaka, Masahiko Saito, Tomoyuki Koganezawa, Kazuo Takimiya, Adv. Mater. 26 (2014) 331.
[16] Ergang Wang, Jonas Bergqvist, Koen Vandewal, Zaifei Ma, Lintao Hou, Angelica Lundin, Scott Himmelberger, Alberto Salleo, Christian Muller, Olle Inganäs, Fengling Zhang, Mats R. Andersson, Adv. Energy Mater. 3 (2013) 806.
[17] Zhenhui Chen, Ping Cai, Lianjie Zhang, Yongxiang Zhu, Xiaofeng Xu, Jiangman Sun, Jun Huang, Xuncheng Liu, Junwu Chen, Hongzheng Chen, Yong Cao, J. Polym. Sci., A: Polym. Chem. 51 (2013) 4966.
[18] Pei-Tzu Wu, Felix S. Kim, Richard D. Champion, Samson A. Jenekhe, Macromolecules 41 (2008) 7021.
[19] Erjun Zhou, Junzi Cong, Keisuke Tajima, Kazuhito Hashimoto, Chem. Mater. 22 (2010) 4890.
[20] Chih-Ping Chen, Yi-Chun Chen, Chao-Ying Yu, Poylm. Chem. 4 (2013) 1161.
[21] Mohammed S. Almeataq, Hunan Yi, Solyman Al-Faifi, Abdulaziz A.B. Alghamdi, Ahmed Iraqi, Nicholas W. Scarratt, Tao Wang, David G. Lidzey, Chem. Commun. 49 (2013) 2252.
[22] Mirko Seri, Margherita Bolognesi, Zhihua Chen, Shaofeng Lu, Wouter Koopman, Antonio Facchetti, Michele Muccini, Macromolecules 46 (2013) 6419.
[23] Kwan Wook Song, Ho Jun Song, Tae Ho Lee, Soo Won Heo, Doo Kyung Moon, Polym. Chem. 4 (2013) 3225.
[24] Zaifei Ma, Ergang Wang, Markus E. Jarvid, Patrik Henriksson, Olle Inganäs, Fengling Zhang, Mats R. Andersson, J. Mater. Chem. 22 (2012) 2306.
[25] John Jun-An Chen, Teresa L. Chen, BongSoo Kim, Daniel A. Poulsen, Justin L. Mynar, M.J. Jean, Frechet Biwu Ma, ACS Appl. Mater. Interfaces 2 (2010) 2679.
[26] Pengcheng Zhou, Zhi-Guo Zhang, Yongfang Li, Xingguo Chen, Jingui Qin, Chem. Mater 26 (2014) 3495.
[27] Ho-Jun Song, Doo-Hun Kim, Eui-Jin Lee, Soo-Won Heo, Jang-Yong Lee, Doo-Kyung Moon, Macromolecules 45 (2012) 7815.
[28] Abay Gadisa, Mammo L. Wendimagegn, Mattias Andersson, Shimelis Admassie, Fengling Zhang, Mats R. Andersson, Olle Inganäs, Adv. Funct. Mater. 17 (2007) 3836.
[29] Jang-Yong Lee, Won-Suk Shin, Jung-Rim Haw, Doo-Kyung Moon, J. Mater. Chem. 19 (2009) 4938.
[30] Huan-Hsuan Chang, Che-En Tsai, Yu-Ying Lai, Wei-Wei Liang, So-Lin Hsu, Chain-Shu Hsu, Yen-Ju Cheng, Macromolecules 46 (2013) 7715.
[31] Ming Wang, Xiaowen Hu, Liqian Liu, Chunhui Duan, Peng Liu, Lei Ying, Fei Huang, Yong Cao, Macromolecules 46 (2013) 3950.
[32] Huaxing Zhou, Liqiang Yang, Wei You, Macromolecules 45 (2012) 607.
[33] Xugang Guo, Mark D. Watson, Org. Lett. 10 (23) (2008) 5333.